



Seismic vulnerability of industrial steel structures with masonry infills using a numerical approach

Francesco S. Liguori¹ · Antonio Madeo¹ · Antonio Formisano²

Received: 12 September 2023 / Accepted: 29 September 2023
© The Author(s) 2023

Abstract

Recent earthquakes have highlighted the high vulnerability of the industrial structures that are not specifically designed for accounting seismic forces. Among them, a widespread typology is characterised by steel structures without bracing or other anti-seismic details and with masonry infills. With the aim of increasing the knowledge on the seismic behaviour of these structures, this work focuses on a mechanical-based approach for the evaluation of fragility curves for industrial areas. The exposure data are obtained by in-situ survey and acquiring information available in existing databases, like the Italian Cartis-GL one that is specifically devised for industrial structures. The variability of geometrical and mechanical data and the presence of epistemic uncertainties are considered by constructing a population of structures using the Monte Carlo method. Each structure is analysed through static-nonlinear simulations adopting mixed finite elements accounting for geometrical and constitutive nonlinearities. The approach is tested for infilled steel structures in the industrial area of the municipality of Spezzano Albanese (Italy). Results show that the presence of masonry infill drastically modifies the seismic behaviour of this structural typology. In particular, it turns out that if the mechanical contribution of the infill is neglected, the structures exhibit high damages even for low intensities of the seismic action.

Keywords Seismic vulnerability · Steel structures · Industrial structures · Masonry infills · Fragility curves

✉ Francesco S. Liguori
francesco.liguori@unical.it

Antonio Madeo
antonio.madeo81@unical.it

Antonio Formisano
antoform@unina.it

¹ Department of Informatics, Modelling, Electronics and Systems Engineering DIMES, University of Calabria, Ponte P. Bucci, 87036 Rende, Cosenza, Italy

² Department of Structures for Engineering and Architecture, University of Naples Federico II, Piazzale Tecchio 80, 80125 Naples, Italy

1 Introduction

As demonstrated by the recent earthquakes occurred in different areas of the Italian territory, industrial structures represent a structural typology at high seismic risk (Buratti et al. 2017). In particular, steel structures usually exhibit a better response to seismic action than precast concrete ones (Formisano et al. 2015), as damages produced by Emilia earthquake in 2012 have highlighted (Savoia et al. 2017). However, if designed without any seismic criteria, even steel structures can undergo severe damages and collapses under seismic actions (Formisano et al. 2017). For this reason, recent works are focusing on developing strategies for estimating the seismic vulnerability of steel structures in both residential (Annan et al. 2009; Silva et al. 2020; Nazri et al. 2017) and industrial areas (Formisano et al. 2019, 2022).

Within the framework of urban scale seismic vulnerability estimate, empirical methods, based on input data obtained through observed damages after past earthquakes, are usually adopted (Zuccaro et al. 2020; Li and Chen 2023; Li 2023). Empirical methods provide the probability of occurrence of a certain damage state for varying seismic intensity as discrete damage probability matrices or continuous fragility functions. Usually, this information is given for vulnerability classes, easily recognised to within a building stock. Many empirical methods are available, related to the most frequent structural typologies, as reinforced concrete (Rosti et al. 2021a; Li and Formisano 2023) or masonry (Perelli et al. 2019; Rosti et al. 2021b; Li and Gardoni 2023) buildings.

However, the statistically low number of post-earthquake damage data and the high variability of the typological features of industrial steel structures prevent empirical methods to be used. An alternative is provided by mechanical-based methods (Polese et al. 2008; Rota et al. 2010). As opposite to the empirical ones, these approaches consist in defining numerical models of the structures under consideration which are then analysed to obtain the damage level (D'Ayala and Speranza 2003; Lagomarsino and Giovinazzi 2006; Frankie et al. 2013; Asteris et al. 2014; Simões et al. 2015; Furtado et al. 2016). Uncertainties, that are intrinsically present in empirical methods, need to be explicitly considered and propagated in mechanical models. In fact, random and epistemic uncertainties affect the geometry, the mechanical properties, the seismic action, the damage grades identification and many other aspects involved in the construction of mechanical-based fragility functions (Baker and Cornell 2008). The uncertainties propagation increases the computational cost of the fragility analysis with respect to the analysis of a single building, since numerical simulations need to be repeated many times (Cosenza et al. 2005; Polese et al. 2012). For this reason, the availability of efficient numerical models that allow to reduce the computational cost is of great importance.

The construction of the numerical models can be performed in different ways. One option is to select some index buildings, namely actual buildings taken as representative of a class. In such a case, the advantage is that the analysis is conducted on real buildings, but on the other hand, the proper selection of the index buildings is not an easy task and can significantly influence the results of the vulnerability analysis. Alternatively, it is possible to refer to the so called archetype buildings, ideal representation of the building stock (Leggieri et al. 2021; Ruggieri et al. 2022). In this case, parametric models are constructed and the relevant parameters are changed within properly tuned ranges of variations to cover the possible configurations of the real structures. Other approaches for large scale vulnerability analyses are worth mentioning, as the

hybrid methods that combine empirical observation and mechanical analyses (Kappos et al. 2006), or vulnerability analyses using machine learning techniques (Ruggieri et al. 2021).

One of the main advantages provided by mechanical-based approaches over the empirical ones is represented by the possibility of considering structural typologies for which little post-earthquake real damages are available. This is the case of industrial steel structures, for which mechanical-based fragility curves have been recently proposed by Formisano et al. (2019, 2022).

A relevant aspect to be considered in vulnerability analyses conducted on relatively large areas is represented by the data required for their application. In Italy a recent project carried out by Italian Civil Protection and many Italian universities are being devoted to collecting typological data using the Cartis form (Zuccaro et al. 2015; Zuccaro et al. 2023). In its database (Cartis 2024), many relevant information on building typologies are available regarding both large areas, called compartments, and single structures. Thanks to its features, Cartis form has been recently used in medium-large territorial scale vulnerability analyses (Olivito et al. 2021; Formisano et al. 2021; Sandoli et al. 2022; Chieffo et al. 2021). Interestingly, Cartis database also includes information on industrial structures by the Cartis long-span (GL) form. The effort in collecting data using Cartis GL form remarks the interest of civil protection departments on the vulnerability of these structural typologies and provides many information of reliable vulnerability assessment strategies.

Among the long-span industrial structures, a quite widespread typology is represented by steel structures designed without any seismic criteria and characterised by the total absence of bracings, but with masonry infill along the entire perimeter. As it is well known, infill provide a certain resistance to horizontal actions (Di Sarno et al. 2021) and therefore likely represent the main seismic resistant structural component for this typology. In fact, secondary elements, can play a significant role on the fragility of civil (Uva et al. 2012) and industrial (Babič and Dolšek 2016) buildings. However, to the best of the authors' knowledge, no specific study is available in the literature to assess their seismic vulnerability.

Starting from the premises discussed above, this work focuses on the seismic vulnerability of industrial steel structures with masonry infills. Since no sufficient empirical data are available for this structural typology, a mechanical-based approach is adopted. The starting point is the exposure analysis conducted by using the CARTIS-GL form (Formisano et al. 2022). Then, Finite Element (FE) models are constructed, considering both geometrical and material nonlinearities. Geometrical nonlinear phenomena can be relevant in the seismic behaviour of many structural typologies characterised by high slenderness ratios, as pallet racks (Ungureanu et al. 2016; Tsarpalis et al. 2022) or silos (Khalil et al. 2023). In fact, slender structures under the seismic forces can exhibit stability loss and collapses due to buckling phenomena, as it can be observed from pictures of post-earthquake damages in Clifton et al. (2011), Formisano et al. (2017), Faggiano et al. (2009).

Parametric analyses are conducted to recognise the influence of geometrical and mechanical features on the seismic behaviour. Finally, mechanical-based fragility curves are constructed and the role played by masonry infills is highlighted. Fragility curves are evaluated using a full-blown Monte Carlo method, considering the variability of the structural features observed in the studied area (Liguori et al. 2023). Finally, the approach is tested on the steel structures in the industrial area of Spezzano Albanese, in Southern Italy, where this structural typology has been found extensively.

The work is organised as follows. The numerical model for the analysis of nonlinear beams is presented in Sect. 2. The mechanical-based approach for the evaluation of the fragility

curves is described in Sect. 3. The application of the procedure to the industrial area of Spezzano Albanese is shown in Sect. 4. Finally, conclusions are drawn in Sect. 5

2 Numerical model

The structure is modelled using plane beam FE. In particular, a shear deformable mixed assumed stress FE (Garcea et al. 2012) is used in which displacements and generalised stresses are considered as primary variables. The assumed stress interpolation satisfies equilibrium equations for zero bulk loads (Liguori and Madeo 2021). An elastic-perfectly plastic behaviour is assumed for steel members and the yield surface is represented by an ellipsoid to efficiently consider axial-flexural interaction. The accuracy of the representation of the yield surface can be readily improved by adopting techniques based on the Minkowsky sum of ellipsoids (Magisano et al. 2018). Plasticity is checked at 3 Gauss-Lobatto points on each FE and the integration of the constitutive equation is performed at the element level in order to preserve the assumed stress interpolation (Magisano and Garcea 2020; Liguori et al. 2022).

Masonry infills are modelled by adopting a simple single equivalent strut behaviour, even if more complex model can be used to improve accuracy (Yekrangnia and Mohammadi 2017; Gentile et al. 2019). A backbone uniaxial response is adopted (Cavaleri et al. 2014; Cavaleri and Di Trapani 2014).

Columns are supposed to be fully clamped on foundations. The model has been validated by comparing the results of simple benchmark with those obtained using the commercial FE software SAP 2000 (Computer and Structures 2010) and Abaqus (Hibbit and Sorenson 2007) which are not reported here for brevity. Because of the peculiar structural typology characterised by a symmetric geometry, the assumed planar behaviour with no torsional effect can be certainly accepted. However, in the general case of more complex stiffness and mass distributions, the proposed model ought to be enhanced by considering a three dimensional behaviour.

2.1 Static nonlinear analysis

The equilibrium condition of a structure subject to gravitational loads \mathbf{p}_0 and seismic forces \mathbf{p} , is expressed as

$$\mathbf{s}[\mathbf{d}] - \mathbf{p}_0 - \lambda \mathbf{p} = \mathbf{0} \tag{1}$$

where λ is a load multiplier and $\mathbf{s}[\mathbf{d}]$ is the internal force vector.

Equation (1) is usually solved by means of a continuation method which gives a sequence of equilibrium points, with coordinates $\mathbf{z} = \{\mathbf{d}, \lambda\}$, forming the so-called equilibrium path or capacity curve. While a deeper discussion can be found elsewhere (Magisano and Garcea 2020; Liguori et al. 2022), only a little background is given herein.

Starting from a known equilibrium point $\mathbf{z}_0 \equiv \mathbf{z}^{(n)}$, a new state $\mathbf{z}^{(n+1)}$ is obtained by solving, through a Newton iteration, the following system representing the equilibrium equations plus the arc-length constraint for an assigned value of $\Delta\xi$

$$\begin{cases} \mathbf{r}[\mathbf{d}, \lambda] \equiv \mathbf{s}[\mathbf{d}] - \lambda \mathbf{p} = \mathbf{0} \\ r_\lambda[\mathbf{d}, \lambda] \equiv \mathbf{n}_z^T \mathbf{M}_z(\mathbf{z} - \mathbf{z}_0) - \Delta\xi = 0 \end{cases} \quad \text{with} \quad \Delta\xi \equiv \mathbf{n}_z^T \mathbf{M}_z(\mathbf{z}_1 - \mathbf{z}_0). \tag{2}$$

where \mathbf{z}_1 is the first predictor. The most used and effective arc-length equation is a moving hyperplane having normal vector $\mathbf{n}_z = \{\mathbf{n}, n_\lambda\}$ and metric matrix $\mathbf{M}_z = \text{diag}[\mathbf{M}, \mu]$. Letting

$$\mathbf{K} = \frac{\partial s[\mathbf{d}]}{\partial \mathbf{d}} \tag{3}$$

evaluated as assemblage of element matrices \mathbf{K}_e , Newton iterations are applied to the extended nonlinear system of Eq. (2), giving a sequence of estimates

$$\Delta \mathbf{z}_{j+1} = \Delta \mathbf{z}_j + \dot{\mathbf{z}}_j \quad \text{and} \quad \mathbf{z}_{j+1} = \mathbf{z}_0 + \Delta \mathbf{z}_j$$

where $\Delta = (\cdot)^{(n+1)} - (\cdot)^{(n)}$ represents the difference between quantities at step $n + 1$ and n and the correction $\dot{\mathbf{z}}_j$ is evaluated as

$$\begin{cases} \mathbf{K}_j \dot{\mathbf{d}} - \dot{\lambda} \mathbf{p} = -\mathbf{r}_j \\ \mathbf{n}^T \mathbf{M} \dot{\mathbf{d}} + \mu n_\lambda \dot{\lambda} = -r_{\lambda j} \end{cases} \Rightarrow \begin{cases} \dot{\mathbf{d}} = -\mathbf{K}_j^{-1} (\mathbf{r}_j - \dot{\lambda}_j \mathbf{p}) \\ \dot{\lambda} = \frac{r_{\lambda j} - \mathbf{n}^T \mathbf{M} \mathbf{K}_j^{-1} \mathbf{r}_j}{\mathbf{n}^T \mathbf{M} \mathbf{K}_j^{-1} \hat{\mathbf{s}}_j - \mu n_\lambda} \end{cases}$$

The internal force vector at each iteration, s^j , is evaluated by assembling the contribution of each element s_e . The solution of Eq.(2) is carried out with a global scheme in only displacement variables, while the stresses are maintained at the element level only and evaluated using a return mapping scheme.

2.2 Beam finite element

The steel members are modelled using a beam FE with constitutive and geometrical nonlinearities. We adopt the 2D beam model (Pignataro et al. 1982; Salerno and Lanzo 1997; Garcea et al. 1999) based on the following spatial strain measure

$$\mathbf{e} = \begin{bmatrix} \varepsilon \\ \gamma \\ \chi \end{bmatrix}, \quad \begin{cases} \varepsilon = 1 + u_{,s} - \cos \varphi \\ \gamma = w_{,s} - \sin \varphi \\ \chi = \varphi_{,s} \end{cases} \tag{4}$$

where u , w and φ represent the axial displacement, the transversal displacement and the rotation, respectively, s is an abscissa along the beam axis and a comma indicates derivative. The displacement fields are interpolated using 3 nodes, located at FE ends and at midspan as

$$\mathbf{d}[s] = \begin{bmatrix} u \\ w \\ \varphi \end{bmatrix} = \mathbf{N}_d[s] \mathbf{d}_e, \tag{5}$$

where $\mathbf{d}_e = [u_i, w_i, \varphi_i, u_j, w_j, \varphi_j, \varphi_k]^T$ are the nodal displacements, being i and j the end nodes. For the node k located at midspan only the rotation is considered as degree of freedom. The assumed displacement interpolation is linear for the translations u and w and quadratic for the rotations. Then, the interpolation matrix $\mathbf{D}[s]$ becomes

$$N_d[s] = \begin{bmatrix} \frac{l-s}{l} & 0 & 0 & \frac{s}{l} & 0 & 0 & 0 \\ 0 & \frac{1-s}{l} & 0 & 0 & \frac{s}{l} & 0 & 0 \\ 0 & 0 & \frac{(l-s)(l-2s)}{l^2} & 0 & 0 & \frac{-s(l-2s)}{l^2} & \frac{4s(l-s)}{l^2} \end{bmatrix} \tag{6}$$

where l is the beam's length.

The first variation of the geometrically nonlinear strains $\mathbf{e} = \mathbf{e}[\mathbf{d}_e]$ can be expressed as

$$\delta \mathbf{e}[\mathbf{d}_e] = \mathbf{B}_e[\mathbf{d}_e] \delta \mathbf{d}_e, \tag{7}$$

where $\mathbf{B}_e[\mathbf{d}_e]$ is a compatibility operator.

A mixed assumed-stress interpolation is adopted, namely stresses are also assumed as primary variables. Then, the generalised stresses, work-conjugate to \mathbf{e} , are interpolated as

$$\mathbf{t}_s = \begin{bmatrix} H \\ V \\ M \end{bmatrix} = \mathbf{N}_\beta \boldsymbol{\beta} \tag{8}$$

where H , V and M represent the horizontal resultant, the vertical resultant and the flexural moment, respectively, \mathbf{N}_β is the stress interpolation matrix and $\boldsymbol{\beta}$ are stress parameters. The material stress resultant \mathbf{t} are related to the material ones as

$$\mathbf{t} = \begin{bmatrix} N \\ T \\ M \end{bmatrix} = \mathbf{R}^T \mathbf{t}_s \tag{9}$$

where N and T are normal and shear force, respectively, while \mathbf{R} is a suitable rotation matrix. According to the displacement interpolation, H and V are assumed to be constant, while the flexural moment is linear, namely

$$\mathbf{N}_\beta = \begin{bmatrix} 1 & 0 & 0 & 0 \\ 0 & 1 & 0 & 0 \\ 0 & 0 & 1 & s \end{bmatrix}. \tag{10}$$

The elastic constitutive law is expressed in terms of generalised quantities as

$$\mathbf{e}[s] = \mathbb{F} \mathbf{t}_s[s], \tag{11}$$

where $\mathbb{F} = \text{diag}(EA, EA, EJ)$, where E , A , and J are normal modulus, cross section area and inertia, respectively (Pignataro et al. 1982; Salerno and Lanzo 1997; Garcea et al. 1999).

2.2.1 Linear response

For the linear elastic problem, using a Hellinger-Reissner approach and the assumed displacement and generalised stresses interpolation one obtains

$$\int_{s=0}^l \mathbf{t}_s[s]^T \mathbf{e}[s] ds - \frac{1}{2} \int_{s=0}^l \mathbf{t}_s[s]^T \mathbb{F} \mathbf{t}_s[s] ds - \mathcal{L}_{ext} \equiv \boldsymbol{\beta}_e^T \mathbf{Q}_e \mathbf{d}_e - \frac{1}{2} \boldsymbol{\beta}_e^T \mathbf{H}_e \boldsymbol{\beta}_e - \mathbf{d}_e^T \mathbf{p}_e \tag{12}$$

where \mathcal{L}_{ext} is the work of the element external loads \mathbf{p}_e and \mathbf{H}_e and \mathbf{Q}_e are the element compliance and the compatibility/equilibrium matrices.

From the stationary condition of Eq. (12) one obtains the equilibrium equations and the constitutive laws of the element in discrete generalised format as

$$\begin{cases} \mathbf{H}_e \boldsymbol{\beta}_e - \mathbf{Q}_e \mathbf{d}_e = \mathbf{0} & \forall e \\ \mathbf{Q}_e^T \boldsymbol{\beta}_e - \mathbf{p}_e = \mathbf{0} \end{cases} \quad (13)$$

The stresses can be obtained from the first of Eq. (13) at the FE level and then substituted into the equilibrium equation to obtain a pseudo-displacement format

$$\mathbf{K}_{e0} \mathbf{d}_e = \mathbf{p}_e, \quad (14)$$

where \mathbf{K}_{e0} is the element stiffness matrix. It is worth noting that the equilibrium condition in Eq. (14) has the same format than in usual displacement-based formulations and the stress parameters are evaluated only at the element level.

2.2.2 Constitutive nonlinear law

An elastic perfectly-plastic behaviour is adopted for the steel beam. Plastic admissibility is checked at some Integration Points (IG), located at the midspan and at the two ends at coordinates s_g . The yield function $f[t[s_g]]$ is adopted, defined in the space of the axial force N and bending moment M , while an elastic behaviour of shear force is assumed. The yield surface is described by a Minkowski sum of ellipsoids, as proposed in a general 3D case elsewhere (Magisano et al. 2018). For the purposes of constructing vulnerability curves, when many analyses needs to be executed, the use of only one ellipsoid provides a good compromise between accuracy and efficiency. In such a case, the plastic admissibility condition on the cross section s_g becomes

$$f[t_g] = \mathbf{t}_g^T \mathbf{C}_g \mathbf{t}_g - 1 \leq 0 \quad (15)$$

where for simplicity $\mathbf{t}_g = \mathbf{t}[s_g]$ and

$$\mathbf{C}_g = \begin{bmatrix} 1/N_y^2 & 0 & 0 \\ 0 & 0 & 0 \\ 0 & 0 & 1/M_y^2 \end{bmatrix} \quad (16)$$

in which N_y and M_y are axial force and flexural moment at yielding. If one wants to increase the accuracy in the evaluation of the yield surface, it is possible to adopt more ellipsoids (Magisano et al. 2018).

On the basis of a strain-driven formulation, the stress update is obtained by using a backward Euler scheme for integrating the constitutive law, where the stresses become an implicit function of the assigned strain (displacement) increment. For a mixed FE, the weak form of the finite step constitutive relations over the element becomes

$$\begin{cases} \mathbf{H}_e(\boldsymbol{\beta}_e - \boldsymbol{\beta}_e^{(n)}) + \sum_g \mu_g \frac{\partial f_g}{\partial \boldsymbol{\beta}_e} = \Delta \boldsymbol{\epsilon}_e \\ \mu_g \geq 0 \quad f_g \leq 0 \quad \mu_g f_g = 0 \end{cases} \quad (17)$$

where we assume to test the plastic admissibility conditions in a discrete number of IP identified by the subscript g , $\Delta = (\cdot)^{(n+1)} - (\cdot)^{(n)}$ represents the difference between quantities at step $n + 1$ and n , f is the yield function, and μ_g are the positive plastic multipliers. The quantity ϵ_e is work-conjugate to β_e and can be obtained as

$$\epsilon_e = \sum_g N_{ig}^T \Delta e_g w_g, \tag{18}$$

where g is the numerical integration weight. The superscript $(n + 1)$ is omitted to simplify the notation.

This problem, is solved by adopting the dual decomposition approach presented elsewhere (Magisano and Garcea 2020; Liguori et al. 2022) which is based on the solution of two sub-problems. The first regards only IP variables and consist in obtaining $t_g = t_g[t_g^{(n)}, \Delta e_g]$ for assigned Δe_g , by solving the following equations

$$\begin{cases} \mathbb{F}_g(t_g - t_g^{(n)}) + \mu_g \frac{\partial f_g[t_g]}{\partial t_g} - \Delta e_g = \mathbf{0} \\ \mu_g f_g[t_g] = 0 \quad \mu_g \geq 0 \quad f_g[t_g] \leq 0 \end{cases} \quad \forall g, \tag{19}$$

which represent a well-known scheme solved in displacement-based formulations.

The second problem, referred to as element state determination, consists in obtaining $\beta_e = \beta_e[\beta_e^{(n)}, \Delta \mathbf{d}_e]$ for assigned $\Delta \mathbf{d}_e$ by solving the following equations regarding elemental variables

$$\begin{cases} \mathbf{r}_g = t_{sg} - N_{ig} \beta_e = \mathbf{0} \quad \forall g \\ \mathbf{r}_e = \Delta \epsilon_e - \sum_g N_{ig}^T \Delta e_g w_g = \mathbf{0} \end{cases} \tag{20}$$

where the unknowns are β_e and $\Delta \epsilon_e$ and $t_{sg} = t_s[s_g]$.

Finally, it is possible to obtain the element force vector as

$$\mathbf{s}_e = \mathbf{Q}_{te}[\mathbf{d}_e]^T \beta_e, \tag{21}$$

where the tangent compatibility operator $\mathbf{Q}[\mathbf{d}_e]$ can be obtained as

$$\mathbf{Q}_{te}[\mathbf{d}_e] = \frac{\partial \epsilon[\mathbf{d}_e]}{\partial \mathbf{d}_e} = \sum_g N_{ig}^T \mathbf{B}_g[\mathbf{d}_e] w_g \tag{22}$$

By adopting well-known procedures, it is possible to evaluate the element stiffness matrix \mathbf{K}_e .

2.2.3 Masonry infill

The masonry infill is modelled using an equivalent strut model. Therefore, only axial deformation in small displacements is considered, namely

$$\mathbf{e} = \begin{bmatrix} \epsilon \\ 0 \\ 0 \end{bmatrix}, \quad \epsilon = u_{,s}. \tag{23}$$

Accordingly, the axial force N is the only generalised force. The equivalent strut has width w_m evaluated through the expression proposed by Papia et al. (2003)

$$w_m = dk \frac{c}{z} \frac{1}{(\lambda^*)^\beta} \tag{24}$$

where $k = l/h$, while c and β depend on Poisson’s ratio ν_d along the diagonal direction (Cavaleri et al. 2014)

$$\begin{aligned} c &= 0.249 - 0.0116\nu_d + 0.569\nu_d^2 \\ \beta &= 0.146 - 0.0073\nu_d + 0.126\nu_d^2. \end{aligned} \tag{25}$$

The parameter λ^* is obtained as

$$\lambda^* = \frac{E_m t_m h'}{E A_c} \left(\frac{h'^2}{l'^2} + \frac{A_c l'}{4A_b h'} \right) \tag{26}$$

where E_m and E are masonry and steel Young modulus, respectively, A_c and A_b are the area of columns and beam, respectively, t_m is the thickness while h' , l' are frame height and length.

A backbone curve is used to describe the infill nonlinear behaviour, as indicated in Fig. 1, providing the axial force as a function of the stress, namely $N = N[\varepsilon[\mathbf{d}_e]]$. The characteristic points having strain ε_1 , ε_2 and ε_3 and axial force N_1 , N_2 and N_3 are evaluated according to (Cavaleri and Di Trapani 2014).

2.3 Damage levels

Nonlinear static analyses are performed on the FE model to simulate the seismic response. An arc-length algorithm is employed to trace the equilibrium path (Liguori et al. 2022).

Figure 9 shows the capacity curves obtained both for the infilled structure and the bare one. It is possible to observe that the presence of the masonry infill increases the initial stiffness and the peak shear force (T). After peak, a strong degradation is observed and the infills contribution vanishes, so that the structural behaviour coincides with that of the bare frame (De Luca et al. 2013).

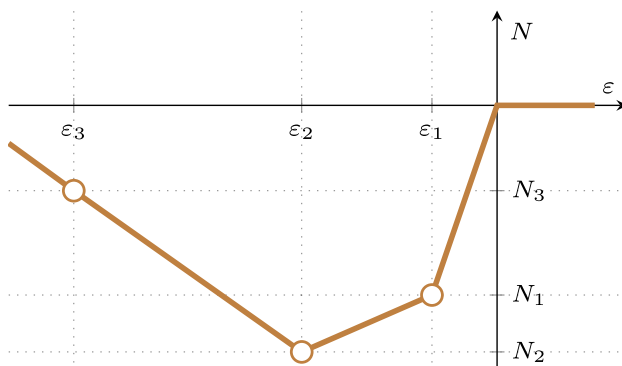


Fig. 1 Backbone curve describing the infill nonlinear behaviour

Three damage levels are considered, namely immediate occupancy (IO), Life Safety (LS) and Near Collapse (NC) (Agency 2013; Formisano et al. 2017, 2022). The damage state is defined in terms of inter-storey drift, on the basis of the FEMA (Agency 2013) legislative provisions, which refers to the following limits: 0.0075 for IO, 0.025 for LS and 0.05 for NC.

Furthermore, a NC limit state is reached when the shear force reaches a limit value $T_y = \frac{f_y}{\sqrt{3}}A_s$, being A_s the shear area, depending of the cross section shape.

3 Mechanical based fragility curves

In this Section, the procedure for constructing the fragility curves using a mechanical-based approach is presented. Its essential steps are summarised in the flowchart in Fig. 2, whose details are given in the following.

3.1 Exposure analysis and data collection

The first step of the proposed approach consists in the data collection of the industrial buildings in the area under consideration. Data can be obtained by exploiting different sources, as the information contained in available database. In the Italian territory, a relevant source is represented by the CARTIS GL form, specifically developed to collect data on large span industrial structures. In particular, the CARTIS GL provides information on material, geometrical features, as height, plan dimensions, number of frames and distance, presence and type of bracing and constraints. In addition, other specific details are provided, as the presence of infill, their typology and regularity. The information are available at two different scales: a wider area containing homogeneous structures and which are

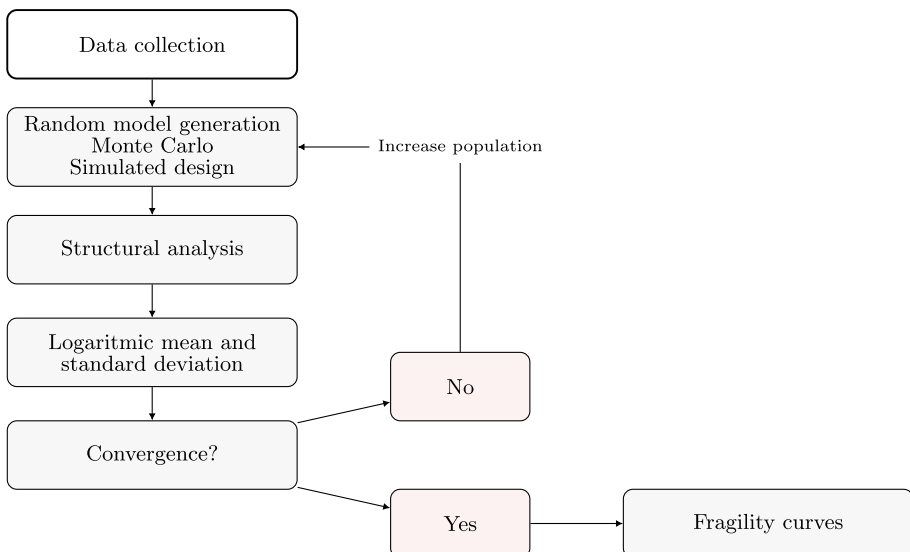


Fig. 2 Flowchart showing the main steps of the mechanical based fragility curves construction method

called compartments, and a specific one at the level of the single structures. In this work, the compartment CARTIS GL form is adopted to identify the area under consideration, while the CARTIS GL at the structural level is used for obtaining the detailed information used in the construction of the fragility curves. It is worth noting that usually not all the structures on a compartment are surveyed, then specific data are available only for a sample of the industrial buildings. The collected parameters and the possible source are summarised in Table 1. In the last two rows, the geometry of the roof and its structure are inserted. In this case, specific surveys are required to identify in detail this information.

However, other data are difficult to estimate, even if detailed surveys are conducted, as the mechanical parameters of the material. In this case, if no specific information can be obtained from original drawings or material tests, material properties are treated as epistemic uncertainties and a wide range of variations are adopted, according to the usual values for the period of construction of the examined structures.

3.2 Parametric models generation

On the basis of the collected data on the industrial buildings under consideration, parametric models are constructed. These models are devised in order to represent the essential features of the family of structures under consideration, even if no actual building is specifically modelled. In the field of seismic vulnerability, these are usually referred to as archetype models Ruggieri et al. (2023). The archetypes are constructed by combining the parameters given in Table 1, which represent the variation of geometrical and mechanical features among the structural typology under consideration. Then, for each archetype a FE model is constructed, as shown in Sect. 2.

The combination of the structural parameters, which define the archetypes, is done using a Monte Carlo technique. A large number of structures is generated by randomly assigning a value to each structural parameter to within observed ranges of variation. If the number of available CARTIS GL forms is statistically relevant, information on the occurrence frequency can be used in the random generation and if not, a uniform variation is assumed. The dimension of the Monte Carlo population needs to be checked by performing a convergence study on the fragility curves, whose construction is described in the following Sections.

Table 1 Parameters collected in the data collection and the possible source

| Data | Source |
|-----------------------------|-----------------------|
| Material | CARTIS GL compartment |
| Number of frames | CARTIS GL |
| Length | CARTIS GL |
| Frame distance | CARTIS GL |
| Height | CARTIS GL |
| Infill material | CARTIS GL |
| Infill regularity (windows) | CARTIS GL |
| Bracing | CARTIS GL |
| Base connection | CARTIS GL |
| Construction year | CARTIS GL |
| Roof geometry | Specific survey |
| Roof truss dimensions | Specific survey |

3.3 Vulnerability model

Each FE model representing an archetype building is subject to static-nonlinear analysis, in order to identify the performance point for the damage levels introduced in Sect. 2.3. The seismic action is represented by the idealised spectra of Newmark–Hall type defined by Italian seismic code (Ministerial Decree 2008). In order to obtain the displacement demand, we make use of the inelastic spectra method. In particular, the modified N2 method (Dolšek and Fajfar 2004, 2005, 2008), specifically devised to be used in presence of masonry infills, is adopted. The analysis is repeated along the two main directions of the structure.

3.4 Fragility curves

Fragility curves are constructed for the structural typology under consideration. As usual (Rota et al. 2010; Liguori et al. 2023; Formisano et al. 2022), fragility curves are expressed by means of cumulative lognormal probability functions of the ground acceleration a_g taken as intensity measure

$$p(d \geq d_i) = \Phi \left(\frac{\log \left(\frac{\lambda_i}{a_g} \right)}{\beta_i} \right), \quad i = 1, \dots, 3, \quad (27)$$

where d is the structural damage (IO, LS, NC), Φ is a normal cumulative probability function, while λ_i and β_i are the mean value and the logarithmic standard deviation of the a_g values that cause the d_i damage grade, respectively. For each damage grade d_i , the definition of a fragility curve requires the evaluation of the two parameters λ_i and β_i on the basis of the results of the analyses conducted.

4 Fragility curves for the industrial area of Spezzano Albanese

In this Section, the mechanical based approach for the evaluation of the seismic fragility curves for infilled industrial steel structures is applied to a case-study concerning the industrial area of Spezzano Albanese.

4.1 Exposure analysis

The area under consideration, indicated in Fig. 3, is located in the municipality of Spezzano Albanese, in Calabria region, southern Italy. It is an industrial area built before 1980 and mainly devoted to agricultural purpose which is the principal economic activity of the zone. The total number of industrial buildings is 48, of which 14 made of steel. The structural data for 11 structures is collected using Cartis-GL form and some of them are given in Table 2.

The structures are composed by a sequence of parallel frames, realised by steel columns and a truss arch. A typical plan view of the industrial structure is shown in Fig. 4.

Fig. 3 Localisation of the studied area

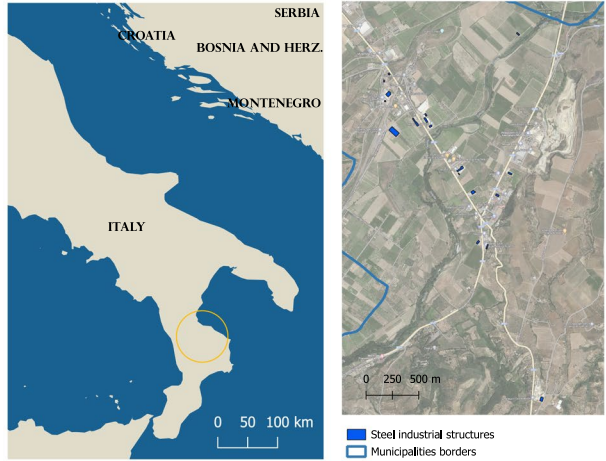


Table 2 Some data collected through the Cartis form for the surveyed industrial structures

| ID | h [m] | h_a [m] | L [m] | n_t | H_i [m] |
|-----|---------|-----------|---------|-------|-----------|
| 101 | 6.6 | 1 | 11.8 | 7 | 5.1 |
| 102 | 6.5 | 1.5 | 15 | 7 | 6.5 |
| 103 | 4.7 | 2 | 12.1 | 7 | 3.7 |
| 104 | 4.6 | 2.8 | 15 | 8 | 3.6 |
| 105 | 4.6 | 2.8 | 15 | 11 | 2.6 |
| 106 | 7.1 | 1.6 | 13.4 | 4 | 5.1 |
| 107 | 4.6 | 0.4 | 11.5 | 8 | 4.6 |
| 108 | 4.5 | 0.5 | 11.7 | 16 | 4.5 |
| 109 | 8.3 | 2.1 | 18.74 | 6 | 8.3 |

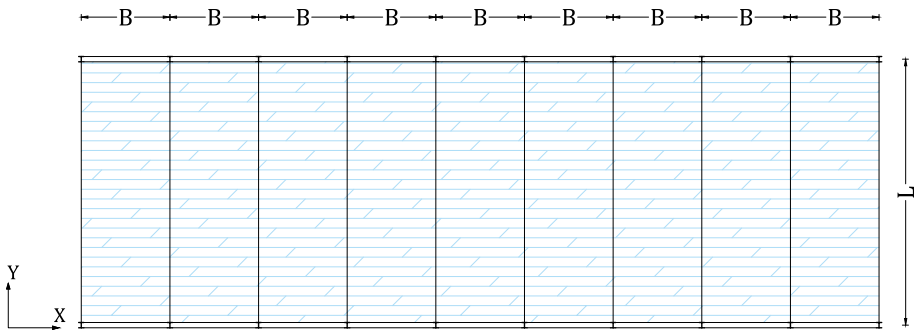


Fig. 4 Plan of an industrial steel structure under consideration

Figure 5 shows some pictures of the industrial steel structures. It is possible to observe how masonry walls are present along the perimeter of the structures. In particular, two configurations are recognised, depending on the walls height, as shown in Fig. 6.



Fig. 5 Some pictures of the industrial structures in the area under consideration. It is possible to observe the geometry of the curved roof truss (a, c, e), the connection between truss and columns (b, f) and a view from the outside (d)

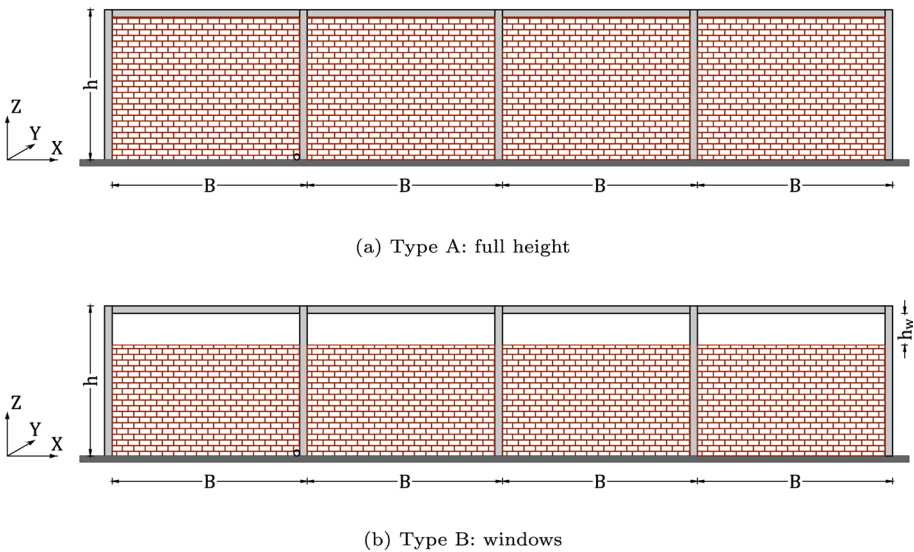


Fig. 6 Full height (a) and windowed (b) infills configurations along x direction

Along y directions, the structures are characterised by a curved truss, as it can be observed in Fig. 5.

Each surveyed structure is characterised by the group of data listed in Table 3 in which their ranges of variations are also given. Based on these parameters, it is possible to construct the archetype models of the industrial structures. Regarding the x direction, a representation is given in Fig. 7. Columns are considered to be fully clamped at the base,

Table 3 Variability of geometrical and mechanical parameters of the recognised industrial buildings

| Parameter | Description | Minimum value | Maximum value |
|-----------|------------------------------|---------------|---------------|
| L | Length | 11 m | 15 m |
| h | Column height | 4.5 m | 7.3 m |
| h_a | Arc height | 0.4 m | 2.8 m |
| h_w | Windows height | 0.7 m | 2.0 m |
| n_r | Number of frames | 4 | 16 |
| B | Frame distance | 5 m | 5 m |
| C_s | Column section (See Table 4) | 1 | 13 |
| B_s | Beam section (See Table 5) | 1 | 11 |

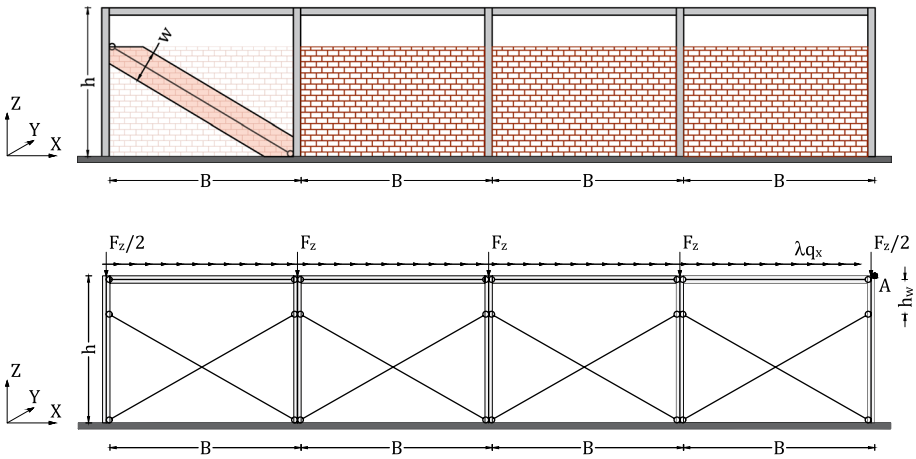
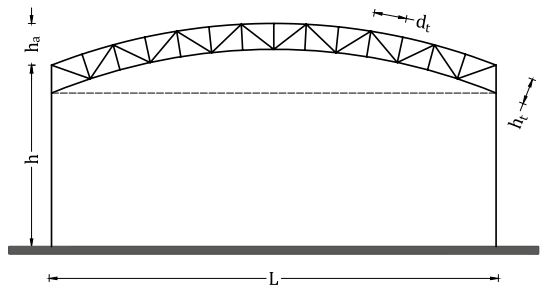


Fig. 7 Geometric and FE parametric model of an infilled frame along x direction

Fig. 8 FE parametric model along y direction



while rotation is allowed in the connection between column and beams. Figure 8 shows the model of the archetype industrial building along y direction. Also along this direction columns are clamped at the base, while the other trusses are hinged to each other. The geometrical parameters vary to within the ranges given in Table 3. Column and beam sections are indicated through an index, as shown in Tables 4 and 5.

Table 4 Section types used for columns

| | | | | | | | | | | | | |
|-------------|------|------|------|------|------|------|------|------|------|------|------|--|
| Index | 1 | | 2 | | | | | | | | | |
| Section-IPE | 270 | | 300 | | | | | | | | | |
| Index | 3 | 4 | 5 | 6 | 7 | 8 | 9 | 10 | 11 | 12 | 13 | |
| Section-HE | 200A | 220A | 200B | 240A | 220B | 260A | 240B | 280A | 260B | 300A | 280B | |

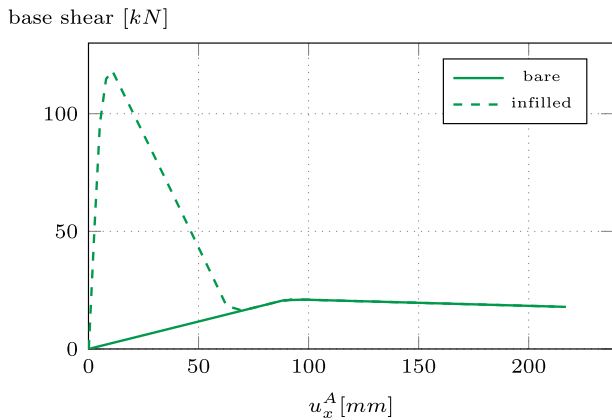
Table 5 Section types used for beams

| | | | | | | | | | | | |
|-------------|-----|-------|-----|-------|-----|-------|-----|-------|-----|-------|-----|
| Index | 1 | 2 | 3 | 4 | 5 | 6 | 7 | 8 | 9 | 10 | 11 |
| Section-IPE | 140 | 160 A | 160 | 180 A | 180 | 200 A | 200 | 220 A | 220 | 240 A | 240 |

Table 6 Variability of additional parameters

| Parameter | Description | Minimum value | Maximum value |
|------------|-------------------------|-----------------------|---------------------|
| σ_y | Steel yield stress | 200 MPa | 350 MPa |
| f_{vt} | Infill shear resistance | 0.1 MPa | 0.3 MPa |
| q | Permanent roof load | 0.3 kN/m ² | 2 kN/m ² |

Fig. 9 Capacity curves for bare and infilled type A frames, x direction



The considered variation allows to cover all the possible configurations obtained from the Cartis GL form. Unfortunately, no information is available with respect to some other parameters, as the steel yield stress, and, therefore, their variation has been assumed to within the reasonable values given in Table 6. The elastic modula are kept constant during the FE simulation. For the steel elements, we consider $E = 210000$ MPa, while for the masonry infill $E_m = 7540$ MPa and $\nu_d = 0.25$.

Finally, the seismic action is described by a Newmark-type response spectrum, evaluated according to Italian building code (Ministerial Decree 2008) for a soil of class C and a topography type T1, as expected in the municipality of Spezzano Albanese.

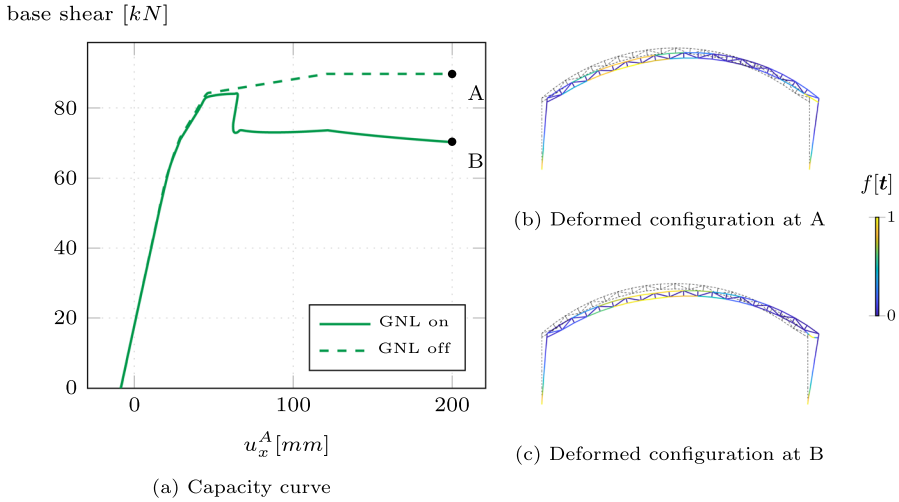


Fig. 10 Capacity curves for seismic action along y direction (a) and deformed configurations at the last evaluated equilibrium point when neglecting (b) and considering (c) geometrical nonlinearities (GNL)

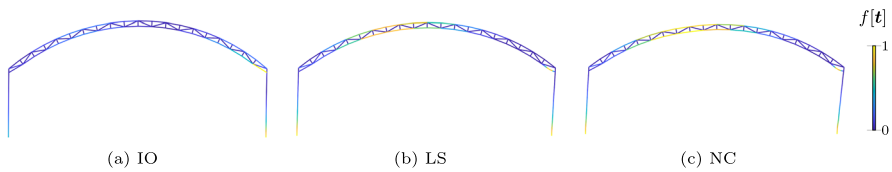


Fig. 11 Deformed configuration and heatmap of the yield function for the reference structure at IO (a), LS (b) and NC (c) limit states, y direction

4.2 Parametric analyses

In this Section, a parametric analysis is presented, with the aim of identifying the influence that each structural parameter has on the seismic capacity of inspected structures. To this aim, a reference structure, characterised by the parameter values given in Table 7, is considered. Starting from these values, sensitivity curves are constructed by varying each parameter and obtaining the seismic intensity, expressed in terms of peak ground acceleration a_g , which produces the damage levels.

Figure 9 shows the capacity curve of the reference building for seismic action along x direction, in both cases of bare frame and infilled type A. The bare frame gives an elastic-perfectly plastic response, with a low softening branch due to the p-delta effect. As expected, the infill increases the initial stiffness and the maximum force with respect to the bare frame case. However, the behaviour is more fragile, with a pronounced softening branch after attainment of the peak the force. For large displacements, when the infill contribution is strongly reduced, the capacity curves of the infilled frame coincides with that of the bare one.

Figure 10 shows, instead, the capacity curve for seismic force along y direction. In particular, two cases are analysed, namely a first one in which geometrical nonlinearities are

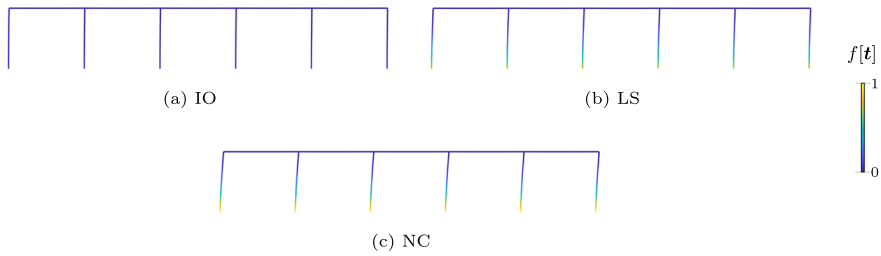


Fig. 12 Deformed configuration and heatmap of the yield function for the reference structure at the IO (a), LS (b) and NC (c) limit states, x direction (bare frame)

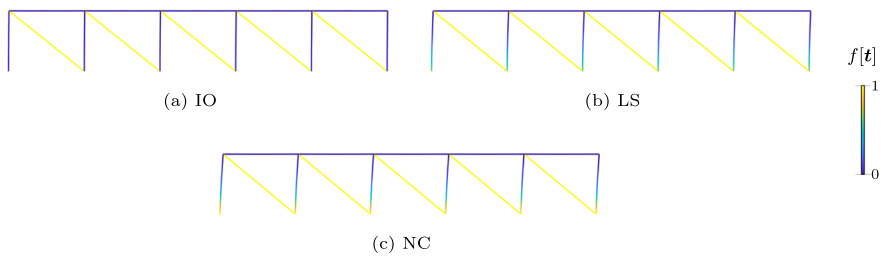


Fig. 13 Deformed configuration and heatmap of the yield function for the reference structure at IO (a), LS (b) and NC (c) limit states, x direction (type A infill)

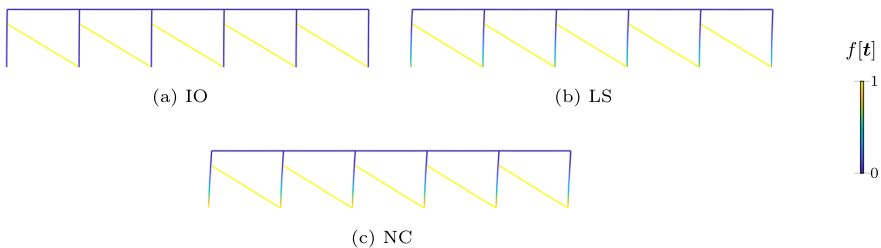


Fig. 14 Deformed configuration and heatmap of the yield function for the reference structure at IO (a), LS (b) and NC (c) limit states, x direction (type B infill)

Table 7 Parameters of the reference structure

| Parameter | L | h | h_w | n_t | B | C_s | B_s | σ_y | f_{vt} | q |
|-----------|------|-----|-------|-------|-----|--------|--------|------------|----------|-----------------------|
| Value | 15 m | 4 m | 1.5 m | 6 | 5 m | HE240A | IPE200 | 275 MPa | 0.2 MPa | 1.5 kN/m ² |

considered and a second one in which their effect is neglected. Results show that in the first case the structure reaches a peak force with a short plastic range, followed by a softening branch. This is due to the instability phenomenon produced by the local buckling of a compressed truss located near the left column, as it can be observed from the deformed configuration at equilibrium point B in Fig. 10. Conversely, if geometrical nonlinearities

are not considered, the model is not capable of capturing this phenomenon, and no softening is observed.

For the reference structure, Fig. 11 shows the deformed configuration for a seismic action along the y direction and a heatmap of the yield function for the three limit states. It is worth noting that at IO yielding occurs at one column base only, while one truss element is near yielding. Then, at LS, both columns base sections are yielded and a local buckling is observed at one truss, while the stresses increase on many elements on the truss structure. Finally, at the most severe limit state, NC, many truss elements reach the yield stress. Similar considerations can be done for a seismic action along the x direction. Figure 12 shows how the yield stress evolves with the limit states in the bare frame case. The collapse mechanism in this case is very simple and involves the base section of the columns. Figures 13 and 14 for the type A and B infills, respectively, show that at IO only the infill is damaged, while the steel members behave elastically. For the more severe limit states, the stress level increases at the columns base sections that reach the yield stress at NC. Interestingly, no relevant difference is observed in the nonlinear structural behaviour between infill types A and B.

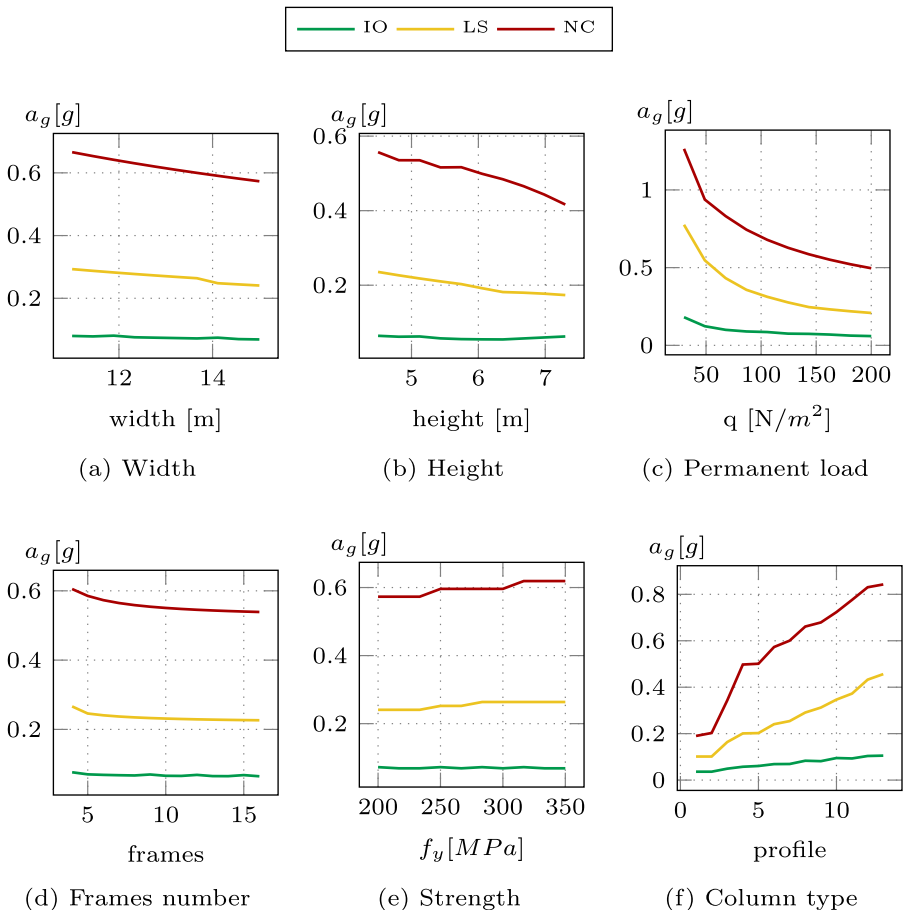


Fig. 15 Sensitivity analysis for some geometrical (a, b, d, f) and mechanical (c, e) attributes, bare frame

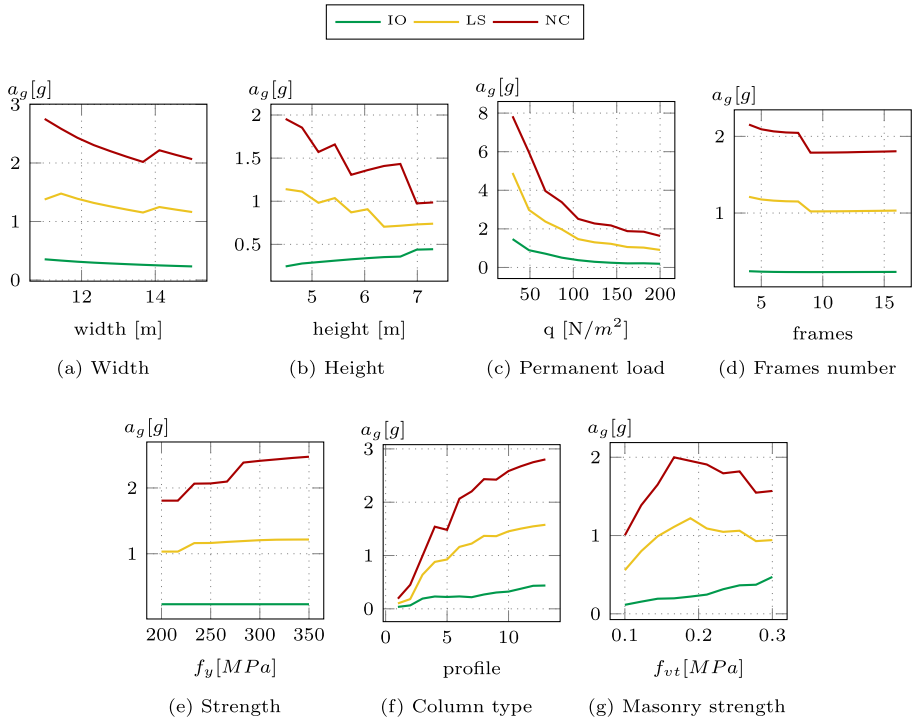


Fig. 16 Sensitivity analysis for some geometrical (a, b, d, f) and mechanical (c, e, g) attributes, type A infills, X direction

Figure 15 shows the sensitivity curves for the case of bare frames. It is possible to observe that high significance is given by the column type, which influence both the elastic and plastic response. Additionally, the permanent load has a high relevance, especially on the damage levels LS and NC, since it influence the total mass of the dynamic system.

Figures 16 and 17 show the sensitivity curves for the infilled frames for the infill types A and B, respectively. In general, one can observe how the a_g values that produce each damage level significantly increase with respect to the bare frame case.

Finally, Fig. 18 shows the results of the parametric study for seismic force along y direction. Again, permanent load and column type turn put to be the most relevant parameters, capable of influencing the seismic response significantly.

4.3 Fragility curves

Fragility curves are obtained by applying the procedure proposed in Sect. 3, based on a Monte Carlo generation of a virtual population of industrial structures. The parameters considered in the variations discussed above are assumed to be equally probable, since no information about more detailed statistics are available. Then, a population of buildings is generated for all the considered infills and seismic directions. The population is increased until a converged value is obtained for logarithmic mean and standard deviation λ and β .

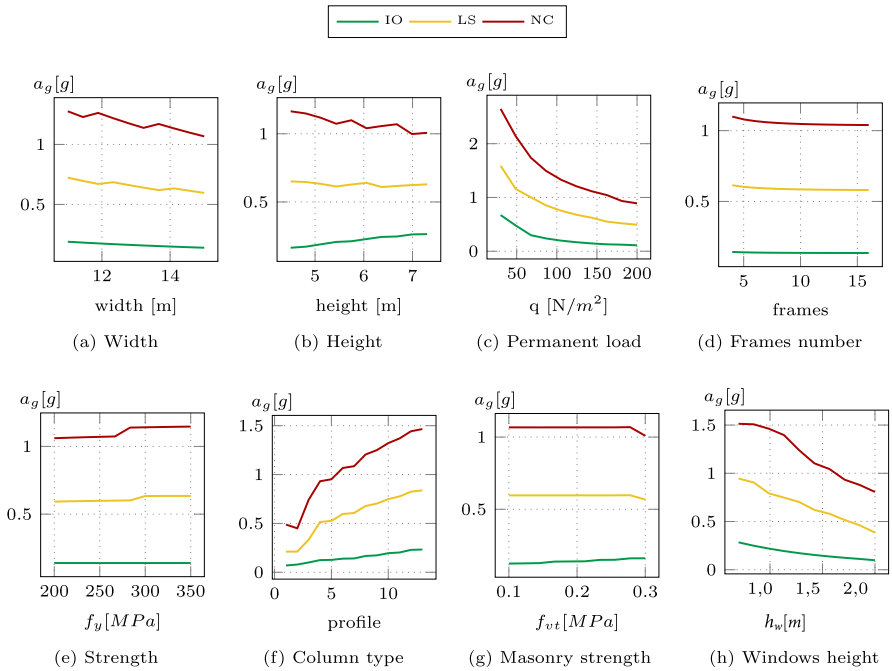


Fig. 17 Sensitivity analysis for some geometrical (a, b, d, f, h) and mechanical (c, e, g) attributes, type B infills, X direction

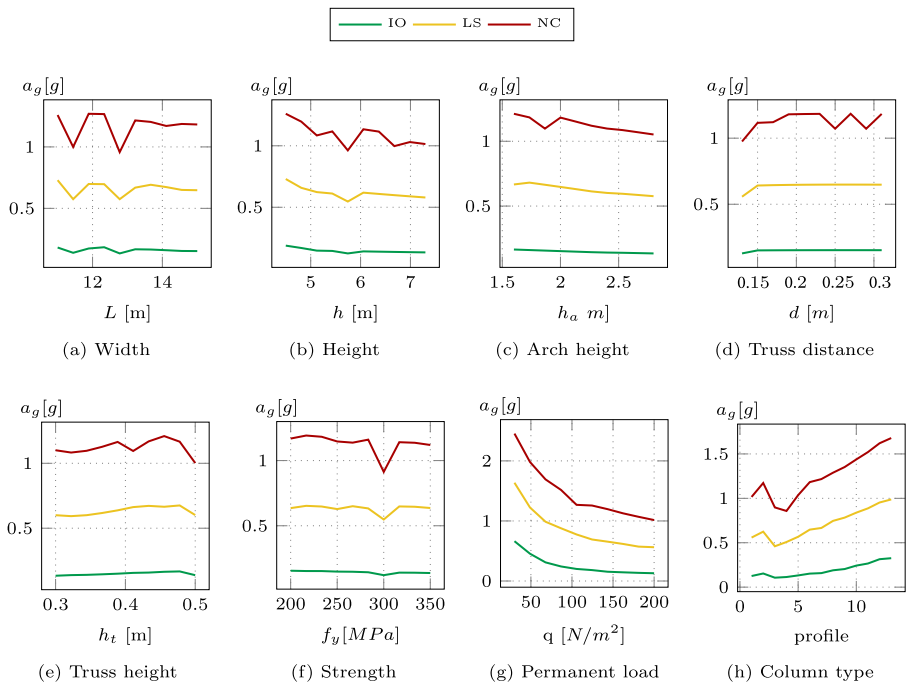


Fig. 18 Sensitivity analysis for some geometrical (a, b, c, d, e, h) and mechanical (f, h) attributes, y direction

Fig. 19 Variation of the parameters λ and β for the fragility curves normalised for the values λ^* and β^* obtained for 10000 buildings, damage level NC, direction x and bare frame

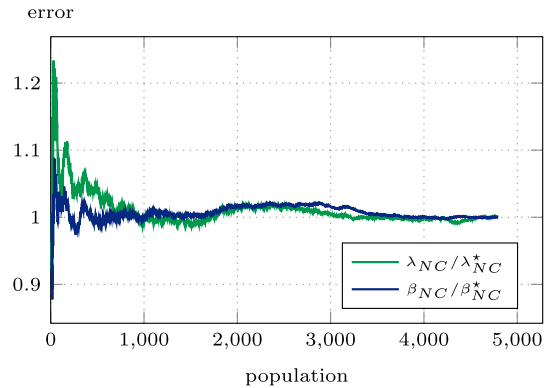


Figure 19 show how these parameters change for increasing population sizes. It is possible to observe how, after a population of about 1000 structures, the values do not change significantly.

Fragility curves are given in Fig. 20. In particular, Fig. 20a shows the fragility curves for bare frame and x direction. In this case, IO damage level is reached for very low intensities of the seismic action. Also the other damage levels are reached for low intensities, thereby highlighting the high vulnerability of steel industrial structures if braces or infills are not present. A completely different behaviour is observed in the infilled case. In fact, as it can be observed in Fig. 20b and c for infill type A and B, respectively, the fragility functions are characterised by high intensity values, with high damage grades having low probability of occurrence even for very high intensities. Then, the presence of the infill drastically modifies the structural behaviour by reducing the seismic vulnerability. Then, it is possible to state that for this type of structure modelling the infill is of crucial importance and suggests that it does not play a secondary structural role, but it behaves as the main seismic-resistant component. However, no relevant difference is observed between the fragility curves for infill type A and B.

Finally, Fig. 20d gives the fragility curves obtained for seismic action along the y direction. In this case, the structures result vulnerable especially to damage grade IO, because for low intensity it has a high probability of occurrence.

For all the analysed cases, the parameters of the lognormal fragility curves are given in Table 8.

5 Concluding remarks

In this work, the problem of the seismic vulnerability of steel industrial structures designed without anti-seismic criteria and with masonry infills was addressed. An exposure analysis of an industrial area in the municipality of Spezzano Albanese (Italy) was conducted using Cartis GL form. A numerical model, based on beam finite elements having geometrical and mechanical nonlinearities was constructed to analyse the industrial structures. On the basis of the surveyed data, sensitivity analysis has been conducted to identify the most relevant parameters. Results have shown that the mass of the construction has a remarkable influence on the seismic vulnerability, thereby suggesting to reduce the weight of the roof to alleviate the seismic risk. By comparing fragility curves for bare and infilled frames, it

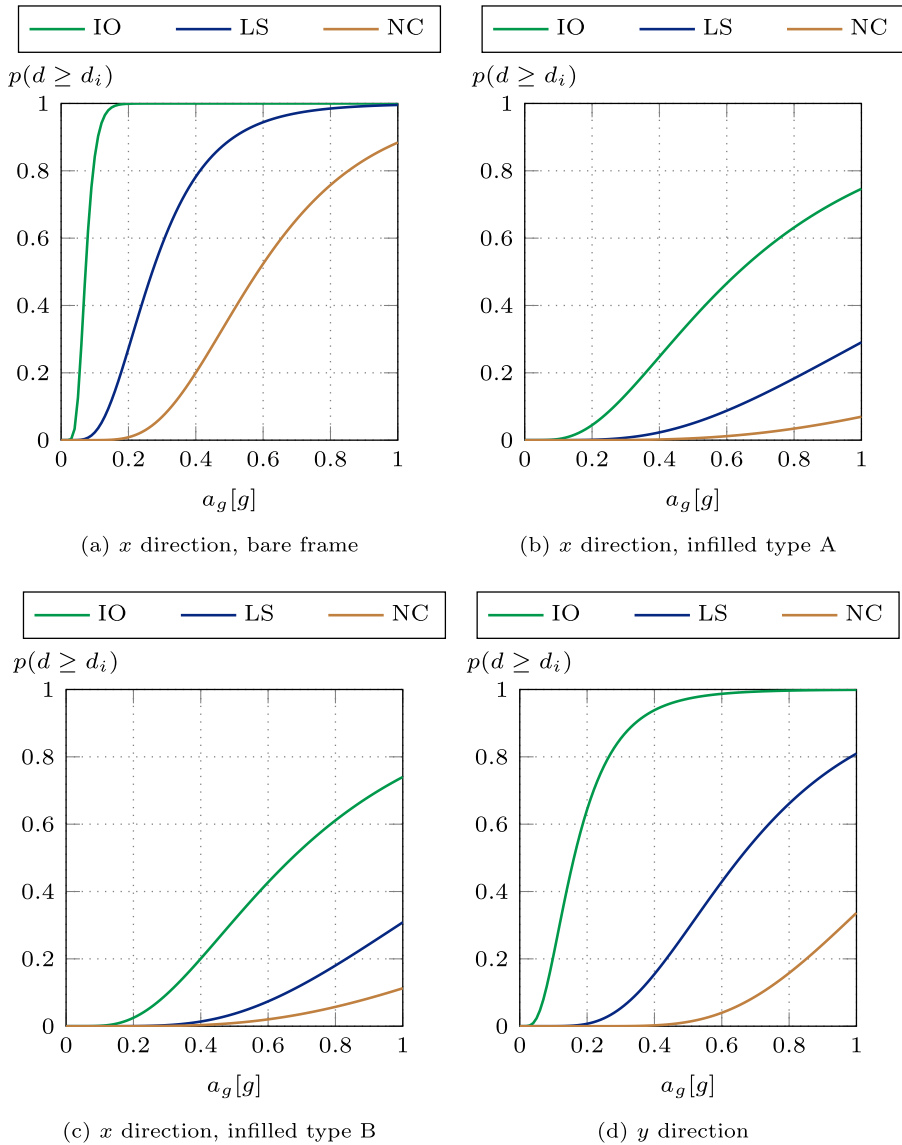


Fig. 20 Fragility curves obtained using the proposed mechanical-based procedure for the industrial steel structures in Spezzano Albanese for seismic action along the *x* direction in the case of bare frame (a), type A infills (b) and type B infills (c) and for seismic action along the *y* direction (d)

was noticed that the presence of masonry infills has a positive influence on the seismic vulnerability of the analysed structures.

Further developments of the study will foresee additional nonlinear dynamic analysis on the examined structures to validate and refine the achieved results.

Table 8 Parameters of the fragility curves

| Case | IO | | LS | | LC | |
|------------------------------|---------------|---------|---------------|---------|---------------|---------|
| | λ [g] | β | λ [g] | β | λ [g] | β |
| x direction, bare frame | 0.072 | 0.322 | 0.271 | 0.500 | 0.584 | 0.450 |
| x direction, infilled type A | 0.636 | 0.681 | 1.420 | 0.635 | 2.627 | 0.653 |
| x direction, infilled type B | 0.672 | 0.618 | 1.310 | 0.539 | 2.100 | 0.612 |
| y direction | 0.161 | 0.590 | 0.654 | 0.484 | 1.176 | 0.383 |

Author contributions FSL: methodology, software, investigation, conceptualisation, original draft AM: supervision, methodology, conceptualisation, reviewing AF: supervision, methodology, conceptualisation, reviewing.

Funding Open access funding provided by Università della Calabria within the CRUI-CARE Agreement. This work was supported by the Civil Protection Department in the framework of the WP2 line CARTIS of the DPC-ReLUIIS research project, which is gratefully acknowledged by the authors.

Data availability The datasets generated during and/or analysed during the current study are available from the corresponding author on reasonable request.

Declarations

Conflict of interest The authors have no relevant financial or non-financial interests to disclose.

Open Access This article is licensed under a Creative Commons Attribution 4.0 International License, which permits use, sharing, adaptation, distribution and reproduction in any medium or format, as long as you give appropriate credit to the original author(s) and the source, provide a link to the Creative Commons licence, and indicate if changes were made. The images or other third party material in this article are included in the article's Creative Commons licence, unless indicated otherwise in a credit line to the material. If material is not included in the article's Creative Commons licence and your intended use is not permitted by statutory regulation or exceeds the permitted use, you will need to obtain permission directly from the copyright holder. To view a copy of this licence, visit <http://creativecommons.org/licenses/by/4.0/>.

References

- Agency F (2013) Prestandard and Commentary for the Seismic Rehabilitation of Buildings (FEMA 356). CreateSpace Independent Publishing Platform, <https://books.google.it/books?id=tb4rnwEACAAJ>
- Annan CD, Youssef MA, Nagggar MHE (2009) Seismic vulnerability assessment of modular steel buildings. *J Earthq Eng* 13(8):1065–1088. <https://doi.org/10.1080/13632460902933881>
- Asteris P, Chronopoulos M, Chrysostomou C et al (2014) Seismic vulnerability assessment of historical masonry structural systems. *Eng Struct* 62–63:118–134. <https://doi.org/10.1016/j.engstruct.2014.01.031>
- Babič A, Dolšek M (2016) Seismic fragility functions of industrial precast building classes. *Eng Struct* 118:357–370. <https://doi.org/10.1016/j.engstruct.2016.03.069>
- Baker JW, Cornell CA (2008) Uncertainty propagation in probabilistic seismic loss estimation. *Struct Saf* 30(3):236–252. <https://doi.org/10.1016/j.strusafe.2006.11.003>
- Buratti N, Minghini F, Ongaretto E et al (2017) Empirical seismic fragility for the precast RC industrial buildings damaged by the 2012 Emilia (Italy) earthquakes. *Earthq Eng Struct Dyn* 46(14):2317–2335. <https://doi.org/10.1002/eqe.2906>
- Cartis (2024) Cartis web application. Front Built Environ. <http://cartis.plinivis.it/backoffice/login.php>
- Cavaleri L, Di Trapani F (2014) Cyclic response of masonry infilled RC frames: experimental results and simplified modeling. *Soil Dyn Earthq Eng* 65:224–242. <https://doi.org/10.1016/j.soildyn.2014.06.016>

- Cavaleri L, Papia M, Macaluso G et al (2014) Definition of diagonal Poisson's ratio and elastic modulus for infill masonry walls. *Mater Struct* 47(1):239–262. <https://doi.org/10.1617/s11527-013-0058-9>
- Chieffo N, Formisano A, Ferreira TM (2021) Damage scenario-based approach and retrofitting strategies for seismic risk mitigation: an application to the historical Centre of Sant'Antimo (Italy). *Eur J Environ Civ Eng* 25(11):1929–1948. <https://doi.org/10.1080/19648189.2019.1596164>
- Clifton C, Bruneau M, MacRae G et al (2011) Steel structures damage from the Christchurch earthquake series of 2010 and 2011. *Bull N Z Soc Earthq Eng* 44(4):297–318. <https://doi.org/10.5459/bnzsee.44.4.297-318>
- Computer and Structures (2010) SAP2000. Advanced 14.2.2 structural analysis program—manual
- Cosenza E, Manfredi G, Polese M et al (2005) A multilevel approach to the capacity assessment of existing RC buildings. *J Earthq Eng* 9(1):1–22. <https://doi.org/10.1080/13632460509350531>
- D'Ayala D, Speranza E (2003) Definition of collapse mechanisms and seismic vulnerability of historic masonry buildings. *Earthq Spectra* 19(3):479–509. <https://doi.org/10.1193/1.1599896>
- De Luca F, Vamvatsikos D, Iervolino I (2013) Near-optimal piecewise linear fits of static pushover capacity curves for equivalent SDOF analysis. *Earthq Eng Struct Dyn* 42(4):523–543. <https://doi.org/10.1002/eqe.2225>
- Di Sarno L, Freddi F, D'Aniello M et al (2021) Assessment of existing steel frames: numerical study, pseudo-dynamic testing and influence of masonry infills. *J Constr Steel Res* 185:106873. <https://doi.org/10.1016/j.jcsr.2021.106873>
- Dolšek M, Fajfar P (2004) Inelastic spectra for infilled reinforced concrete frames. *Earthq Eng Struct Dyn* 33(15):1395–1416. <https://doi.org/10.1002/eqe.410>
- Dolšek M, Fajfar P (2005) Simplified non-linear seismic analysis of infilled reinforced concrete frames. *Earthq Eng Struct Dyn* 34(1):49–66. <https://doi.org/10.1002/eqe.411>
- Dolšek M, Fajfar P (2008) The effect of masonry infills on the seismic response of a four-storey reinforced concrete frame—a deterministic assessment. *Eng Struct* 30(7):1991–2001. <https://doi.org/10.1016/j.engstruct.2008.01.001>
- Faggiano B, Iervolino I, Magliulo G et al (2009) Post-event analysis of industrial structures behavior during L'Aquila earthquake. *Progett Sismica* 3:203–208
- Formisano A, Landolfo R, Mazzolani F (2015) Robustness assessment approaches for steel framed structures under catastrophic events. *Comput Struct* 147:216–228. <https://doi.org/10.1016/j.compstruc.2014.09.010>
- Formisano A, Di Lorenzo G, Iannuzzi I et al (2017) Seismic vulnerability and fragility of existing Italian industrial steel buildings. *Open Civ Eng J* 11:1122–1137. <https://doi.org/10.2174/1874149501711011122>
- Formisano A, Di Lorenzo G, Landolfo R (2019) Non-linear analyses and fragility curves of European existing single-story steel buildings. In: AIP conference proceedings, vol 2116, No (1), p 260020. <https://doi.org/10.1063/1.5114271>, <https://aip.scitation.org/doi/abs/10.1063/1.5114271>
- Formisano A, Chieffo N, Clementi F et al (2021) Influence of local site effects on the typological fragility curves for class-oriented masonry buildings in aggregate condition. *Open Civ Eng J M4*:149–164. <https://doi.org/10.2174/1874149502115010149>
- Formisano A, Meglio E, Di Lorenzo G et al (2022) Vulnerability curves of existing Italian industrial steel buildings designed without seismic criteria. In: Mazzolani FM, Dubina D, Stratan A (eds) Proceedings of the 10th international conference on behaviour of steel structures in seismic areas. Springer International Publishing, Cham, pp 872–880
- Frankie TM, Gencturk B, Elnashai AS (2013) Simulation-based fragility relationships for unreinforced masonry buildings. *J Struct Eng* 139(3):400–410. [https://doi.org/10.1061/\(ASCE\)ST.1943-541X.0000648](https://doi.org/10.1061/(ASCE)ST.1943-541X.0000648)
- Furtado A, Rodrigues H, Arede A et al (2016) Simplified macro-model for infill masonry walls considering the out-of-plane behaviour. *Earthq Eng Struct Dyn* 45(4):507–524. <https://doi.org/10.1002/eqe.2663>
- Garcea G, Salerno G, Casciaro R (1999) Extrapolation locking and its sanitization in Koiter's asymptotic analysis. *Comput Methods Appl Mech Eng* 180(1):137–167. [https://doi.org/10.1016/S0045-7825\(99\)00053-5](https://doi.org/10.1016/S0045-7825(99)00053-5)
- Garcea G, Madeo A, Casciaro R (2012) The implicit corotational method and its use in the derivation of nonlinear structural models for beams and plates. *J Mech Mater Struct* 7(6):509–538. <https://doi.org/10.2140/jomms.2012.7.509>
- Gentile R, Pampanin S, Raffaele D et al (2019) Non-linear analysis of RC masonry-infilled frames using the SLaMA method: part 1—mechanical interpretation of the infill/frame interaction and formulation of the procedure. *Bull Earthq Eng* 17(6):3283–3304. <https://doi.org/10.1007/s10518-019-00580-w>
- Hibbit K, Sorenson P (2007) Abaqus analysis user's manual version 6.7

- Kappos AJ, Panagopoulos G, Panagiotopoulos C et al (2006) A hybrid method for the vulnerability assessment of R/C and URM buildings. *Bull Earthq Eng* 4(4):391–413. <https://doi.org/10.1007/s10518-006-9023-0>
- Khalil M, Ruggieri S, Tateo V et al (2023) A numerical procedure to estimate seismic fragility of cylindrical ground-supported steel silos containing granular-like material. *Bull Earthq Eng*. <https://doi.org/10.1007/s10518-023-01751-6>
- Lagomarsino S, Giovinazzi S (2006) Macroseismic and mechanical models for the vulnerability and damage assessment of current buildings. *Bull Earthq Eng* 4:415–443. <https://doi.org/10.1007/s10518-006-9024-z>
- Leggieri V, Ruggieri S, Zagari G et al (2021) Appraising seismic vulnerability of masonry aggregates through an automated mechanical-typological approach. *Autom Constr* 132:103972. <https://doi.org/10.1016/j.autcon.2021.103972>
- Li SQ (2023) Empirical resilience and vulnerability model of regional group structure considering optimized macroseismic intensity measure. *Soil Dyn Earthq Eng* 164:107630. <https://doi.org/10.1016/j.soildyn.2022.107630>
- Li SQ, Chen YS (2023) Vulnerability and economic loss evaluation model of a typical group structure considering empirical field inspection data. *Int J Disaster Risk Reduct* 88:103617. <https://doi.org/10.1016/j.ijdr.2023.103617>
- Li SQ, Formisano A (2023) Statistical model analysis of typical bridges considering the actual seismic damage observation database. *Arch Civ Mech Eng* 23(3):178. <https://doi.org/10.1007/s43452-023-00720-9>
- Li SQ, Gardoni P (2023) Empirical seismic vulnerability models for building clusters considering hybrid intensity measures. *J Build Eng* 68:106130. <https://doi.org/10.1016/j.jobbe.2023.106130>
- Liguori FS, Madeo A (2021) A corotational mixed flat shell finite element for the efficient geometrically nonlinear analysis of laminated composite structures. *Int J Numer Methods Eng* 122(17):4575–4608. <https://doi.org/10.1002/nme.6714>
- Liguori FS, Madeo A, Garcea G (2022) A dual decomposition of the closest point projection in incremental elasto-plasticity using a mixed shell finite element. *Int J Numer Methods Eng* 123(24):6243–6266. <https://doi.org/10.1002/nme.7112>
- Liguori FS, Fiore S, Perelli FL et al (2023) A mechanical-based seismic vulnerability assessment method with an application to masonry structures in Cosenza (Italy). *Bull Earthq Eng*. <https://doi.org/10.1007/s10518-023-01752-5>
- Magisano D, Garcea G (2020) Fiber-based shakedown analysis of three-dimensional frames under multiple load combinations: mixed finite elements and incremental-iterative solution. *Int J Numer Methods Eng* 121(17):3743–3767. <https://doi.org/10.1002/nme.6380>
- Magisano D, Liguori F, Leonetti L et al (2018) Minkowski plasticity in 3D frames: decoupled construction of the cross-section yield surface and efficient stress update strategy. *Int J Numer Methods Eng* 116(7):435–464. <https://doi.org/10.1002/nme.5931>
- Ministerial Decree (2008) Technical codes for constructions (NTC 2018. Official Gazette of the Italian Republic pp 1–434
- Nazri FM, Tan CG, Saruddin SNA (2017) Fragility curves of regular and irregular moment-resisting concrete and steel frames. *Int J Civ Eng* 16:317–927. <https://doi.org/10.1007/s40999-017-0237-0>
- Olivito RS, Porzio S, Scuro C et al (2021) Inventory and monitoring of historical cultural heritage buildings on a territorial scale: a preliminary study of structural health monitoring based on the CARTIS approach. *Acta IMEKO* 10:57–69
- Papia M, Cavaleri L, Fossetti M (2003) Infilled frames: developments in the evaluation of the stiffening effect of infills. *Struct Eng Mech* 16(6):675–693. <https://doi.org/10.12989/sem.2003.16.6.675>
- Perelli FL, De Gregorio D, Cacace F, et al. (2019) Empirical vulnerability curves for Italian masonry buildings. In: COMPDYN 2019 7th international conference on computational methods in structural dynamics and earthquake engineering
- Pignataro M, Di Carlo A, Casciaro R (1982) On nonlinear beam models from the point of view of computational post-buckling analysis. *Int J Solids Struct* 18(4):327–347. [https://doi.org/10.1016/0020-7683\(82\)90058-0](https://doi.org/10.1016/0020-7683(82)90058-0)
- Polese M, Verderame GM, Mariniello C et al (2008) Vulnerability analysis for gravity load designed RC buildings in Naples-Italy. *J Earthq Eng* 12(sup2):234–245. <https://doi.org/10.1080/13632460802014147>
- Polese M, Ludovico MD, Porta A et al (2012) Damage-dependent vulnerability curves for existing buildings. *Earthq Eng Struct Dyn*. <https://doi.org/10.1002/eqe.2249>
- Rosti A, Del Gaudio C, Rota M et al (2021) Empirical fragility curves for Italian residential RC buildings. *Bull Earthq Eng* 19(8):3165–3183. <https://doi.org/10.1007/s10518-020-00971-4>

- Rosti A, Rota M, Penna A (2021) Empirical fragility curves for Italian URM buildings. *Bull Earthq Eng* 19(8):3057–3076. <https://doi.org/10.1007/s10518-020-00845-9>
- Rota M, Penna A, Magenes G (2010) A methodology for deriving analytical fragility curves for masonry buildings based on stochastic nonlinear analyses. *Eng Struct* 32(5):1312–1323. <https://doi.org/10.1016/j.engstruct.2010.01.009>
- Ruggieri S, Cardellicchio A, Leggieri V et al (2021) Machine-learning based vulnerability analysis of existing buildings. *Autom Constr* 132:103936. <https://doi.org/10.1016/j.autcon.2021.103936>
- Ruggieri S, Calò M, Cardellicchio A et al (2022) Analytical-mechanical based framework for seismic overall fragility analysis of existing RC buildings in town compartments. *Bull Earthq Eng* 20(15):8179–8216. <https://doi.org/10.1007/s10518-022-01516-7>
- Ruggieri S, Liguori FS, Leggieri V et al (2023) An archetype-based automated procedure to derive global-local seismic fragility of masonry building aggregates: META-FORMA-XL. *Int J Disaster Risk Reduct* 95:103903. <https://doi.org/10.1016/j.ijdrr.2023.103903>
- Salerno G, Lanzo AD (1997) A nonlinear beam finite element for the post-buckling analysis of plane frames by Koiter's perturbation approach. *Comput Methods Appl Mech Eng* 146(3):325–349. [https://doi.org/10.1016/S0045-7825\(96\)01240-6](https://doi.org/10.1016/S0045-7825(96)01240-6)
- Sandoli A, Calderoni B, Lignola GP et al (2022) Seismic vulnerability assessment of minor Italian urban centres: development of urban fragility curves. *Bull Earthq Eng* 20(10):5017–5046. <https://doi.org/10.1007/s10518-022-01385-0>
- Savoia M, Buratti N, Vincenzi L (2017) Damage and collapses in industrial precast buildings after the 2012 Emilia earthquake. *Eng Struct* 137:162–180. <https://doi.org/10.1016/j.engstruct.2017.01.059>
- Silva A, Macedo L, Monteiro R et al (2020) Earthquake-induced loss assessment of steel buildings designed to Eurocode 8. *Eng Struct* 208:110244. <https://doi.org/10.1016/j.engstruct.2020.110244>
- Simões A, Milosevic J, Meireles H et al (2015) Fragility curves for old masonry building types in Lisbon. *Bull Earthq Eng* 13:3083–3105
- Tsarpalis D, Vamvatsikos D, Delladonna F et al (2022) Macro-characteristics and taxonomy of steel racking systems for seismic vulnerability assessment. *Bull Earthq Eng* 20(5):2695–2718. <https://doi.org/10.1007/s10518-022-01326-x>
- Ungureanu V, Madeo A, Zagari G et al (2016) Koiter asymptotic analysis of thin-walled cold-formed steel uprights pallet racks. *Structures* 8:286–299. <https://doi.org/10.1016/j.istruc.2016.04.006>
- Uva G, Porco F, Fiore A (2012) Appraisal of masonry infill walls effect in the seismic response of RC framed buildings: a case study. *Eng Struct* 34:514–526. <https://doi.org/10.1016/j.engstruct.2011.08.043>
- Yekrangnia M, Mohammadi M (2017) A new strut model for solid masonry infills in steel frames. *Eng Struct* 135:222–235. <https://doi.org/10.1016/j.engstruct.2016.10.048>
- Zuccaro G, Dolce M, De Gregorio D, et al (2015) La scheda CARTIS per la caratterizzazione tipologico-strutturale dei comparti urbani costituiti da edifici ordinari. valutazione dell'esposizione in analisi di rischio sismico (in italian). 34° Convegno Nazionale GNGTS
- Zuccaro G, Perelli FL, Gregorio DD et al (2020) Empirical vulnerability curves for Italian masonry buildings: evolution of vulnerability model from the DPM to curves as a function of acceleration. *Bull Earthq Eng* 19:1456–1573. <https://doi.org/10.1007/s10518-020-00954-5>
- Zuccaro G, Dolce M, Perelli FL et al (2023) CARTIS: a method for the typological-structural characterization of Italian ordinary buildings in urban areas. *Front Built Environ* 9:1129176. <https://doi.org/10.3389/fbuil.2023.1129176>